BULLETIN OF THE POLISH ACADEMY OF SCIENCES
TECHNICAL SCIENCES, Vol. 67, No. 2, 2019
DOI: 10.24425/bpas.2019.127963

Study of ancient forging devices: 3D modelling and analysis using current computer methods

J.I. ROJAS-SOLA[1]*, J.B. BOUZA-RODRÍGUEZ[2], and A. COMESAÑA-CAMPOS[2]

[1] Department of Engineering Graphics, Design and Projects, University of Jaen, Spain
[2] Department of Engineering Design, University of Vigo, Spain

Abstract. An ancient forging device in Spain has been studied, namely the forge with a waterwheel and air-blowing tube or hydraulic trompe, found near the village of Santa Eulalia de Oscos (province of Asturias, Spain). Three procedures using *ad hoc* methods were applied: 3D modelling, finite element analysis (FEA), and computational-fluid dynamics (CFD). The CFD results indicated the proper functioning of the trompe, which is a peculiar device based on the Venturi effect to take in air. The maximum air volume flow rate supplied to the forge by the trompe was shown to be 0.091 m^3/s, and certain parameters of relevance in the trompe design presented optimal values, i.e. offering maximum air-flow supply. Furthermore, the distribution of stress over the motion-transmission system revealed that the stress was concentrated most intensely in the cogs of the transmission shaft (a kind of camshaft), registering values of up to 7.50 MPa, although this value remained below half of the maximum admissible work stress. Therefore, it was confirmed that the oak wood from which the motion system and the trompe were made functioned properly, as these systems never exceeded the maximum admissible working stress, demonstrating the effectiveness of the materials used in that period.

Key words: forging device, hydraulic trompe, 3D modelling, computational-fluid dynamics, finite element analysis.

1. Introduction

Until the end of the 19th century, traditional Spanish ferrous metallurgy was one of the main motors of economic development in areas having ancient finery forges, where iron mineral was transformed into iron metal. In the 20th century, with the development of blast furnaces, the finery forges ceased to function. In many parts of Spain, the terms finery forge and trip hammer were used interchangeably, both for the iron and the copper forge, although in others the term finery forge was used for the mineral iron and trip hammer for copper [1]. In finery forges, mineral iron was transformed into metal iron in a furnace, where layers of mineral alternated with melting and combustible material, the latter usually being charcoal. This mass was heated by air injection to temperatures of 800 to 1300°C for several days. Afterwards, the slag was sloughed off of this mass by blows of a large drop hammer weighing some 150 to 200 kg. Once the iron metal had been produced, it was roughed and stretched into bars, thus taking its definitive form. Although the resulting wrought iron was of good quality, the industrial yield of the operation was low, since about half the metal was lost in the form of slag [2].

The smelting process took place in a small furnace composed of refractory material in which ground, clean mineral was introduced together with combustible material. At first, this combustible material was wood but was later replaced by charcoal (partially burnt wood) to reach a higher calorific power [3]. Originally, these small furnaces were stoked by natural ventilation or by leather bellows operated by hand. However, this procedure caused a discontinuous air flow that did not result in good combustion and thus failed to reach high temperatures.

When the metal was converted in liquid, the slag was deposited in the bottom due to its greater density and the liquid metal was removed with spoons that were tipped into molds. Afterwards, once solidified, it was heated again and forged by striking it with a drop hammer to give it final form and eliminate impurities (dross).

However, this laborious manufacturing process changed radically when the air-feed system was mechanized in metal furnaces and forges during the Renaissance, with the widespread use of the waterwheel as the driving force. The old hydraulic finery forges are an example of industries devoted to the smelting and forging of iron to manufacture domestic utensils, plowing gear and other agricultural equipment, cauldrons, pans, hinges, locks, and especially nails, using water as the driving force [2, 4]. Thus, waterwheels were used for finery forges to inject air into the furnace through devices called *barquines*, and to move the mallets or drop hammers that forged the metal.

Afterwards the waterwheels incorporated a transmission shaft with teeth as a kind of camshaft, to transmit or convert the circular motion into rectilinear movement that would lift or lower the mallets or trip hammers, although in reality this was the application of technology already known in the transmission of movement, replacing the old system of gear wheel-pinion with cams that, alternating, struck the end of the handle of a mallet or

*e-mail: jirojas@ujaen.es

Manuscript submitted 2018-01-15, revised 2018-06-12 and 2018-07-11, initially accepted for publication 2018-07-16, published in April 2019.

trip hammer [5]. The number of times the drop hammer strikes the anvil depends on the number of turns per minute of the wheel and on the number of cogs, this implicitly depending on the diameter of the wheel and the speed at which the water strikes the wheel, and in turn depending on the height of the falling water from the upper water reservoir or *banzado* (normally 2.5 to 3 m) [2]. Thus, for example, a turn speed of 30 rpm and 5 cogs provided 150 strikes per min [1]. The *barquines*, which at that time constituted an advance with respect to the previous method of blowing air into the forge using manual force also underwent an evolution and were replaced by the hydraulic trompe, which is a more efficient device to inject air, based on the Venturi effect. In a rough estimate of output, to produce 150 kg of wrought iron required loading the furnace with 450 kg of mineral iron and 675 kg of charcoal. The process of mineral-iron reduction lasted for 6 hours in the furnace [2].

The technology of these old forging devices has been studied in a series of ethnographic works, but none from a technical or functional standpoint. Among them appear generic studies on Spanish popular technology [5], on old Spanish inventions and hydraulic factories [2, 3], on cottage iron industry and crafting [4, 6], and on the copper boiler and its trip hammer [1, 7]. The only engineering studies available analyze the failure of a drop hammer [8], and one examines old fulling mills [9], a technology very similar to using the waterwheel, which moves the camshaft to lift two mallets that asynchronously beat cloth held in wooden containers. Unfortunately, no functional analysis is available in the literature for the use of finite element analysis (FEA) or computational-fluid dynamics (CFD), and these two analytical techniques treat a major element not addressed in studies using conventional methods.

Hence, the objective of the present work is to provide a rigorous functional and technical analysis to provide information in detail on the technological facets of this ancient forging device found in Spain. Special attention is placed on the study of the hydraulic trompe, due to the peculiar characteristics of these types of devices and the great technological advance that this represented for the period.

The study consists of the following sections. The forging device is described in detail in Section 2, its historical significance being examined in light of the technology used. The methodological approach is explained in Section 3, particularly regarding the 3D geometry and the CFD and FEA simulation. The results and discussion appear in Section 4 and the conclusions in Section 5.

2. Description of the ancient finery forge

The finery forge chosen for this unprecedented research has been recognized at the national level in Spain for its high heritage value, being located at the ethnographic site of Mazonovo, belonging to the town of Santa Eulalia de Oscos (Asturias province, Spain), on the bank of the Candesa River [10]. It is one of the few such forges surviving in Europe.

The site has been completely restored and rehabilitated for a better understanding of the old process of ferrous metallurgy,

Fig. 1. Mazonovo ethnographic site

the structure housing the finery forge being notable for its good state of conservation, having undergone no great modifications over time (Fig. 1) [11].

In the past, the district of Oscos, where the finery forge is located, was isolated from the rest of Spain due to its difficult access, and therefore today it preserves certain peculiarities of cultural interest, as reflected by the visit of the Spanish king in 2016 to present the site with the *Premio al Pueblo Ejemplar* (Exemplary Town Award) for its sustainable development by combining tradition and modernity and for reconciling nature conservation with economic development.

The forge of Mazonovo, dating to the 18th century, fell into disuse in 1970 but was rehabilitated in 1995. Next to it stands an open waterwheel with 16 paddles and iron bands reinforcing it in different sections (Fig. 2). It has an outside diameter of 2.30 m and a width of 0.22 m solidly connected to an axle or transmission shaft 5.13 m long and 0.40 m in diameter. Both the

Fig. 2. Waterwheel

Fig. 3. Detail of the two pulls for the valves that fill the two vertical conduits

axle and wheel are constructed of oak for its structural quality and its durability.

As can be appreciated, the wheel is activated by water (from the vertical conduit of rectangular section) striking the upper paddles, converting the potential energy of the water stored in the upper reservoir or banzado (the only one of wood in Spain; Fig. 3) into kinetic energy and thereby rotating the waterwheel. The position of an upper feed of the waterwheel as opposed to a lower one is justified because, for realistic parameter values, the overshot wheel is significantly more powerful, particularly for low flow rate and large wheel radius [12].

This in turn rotates the axle or transmission shaft (Fig. 4) fixed to the wheel, converting this angular movement in a rectilinear one of raising and lowering the drop hammer for the

Fig. 4. Detail of the teeth forming the cams (*malobreiros*) and the cooling channel of the transmission shaft supports

metal forge, owing to 4 teeth functioning as cams (*malobreiros*) fixed to the axle. Each of the cams alternately strike the handle of the drop hammer at a point protected by a piece of iron (*xemela*), forcing the handle downwards until it meets a stone embedded in the soil (*tendal*) so that the handle increases the force after the blow of the cam and, consequently, increases power of the action of the drop hammer.

The handle, made of wood, has a length of 2.91 m and an average diameter, given that the cross-section is not regular, of 0.25 m. The hammer, made of wrought iron, weighs 113 kg, has a height of 0.74 m, a length of 0.17 m and a width that varies between 0.09 m at the narrower bottom end and 0.26 m at the thicker top end (Fig. 5).

Fig. 5. Forging process by blows of the drop hammer

As stated previously, the angular velocity of the waterwheel depends on the quantity of water supplied by the vertical conduit and that strikes the paddles; for this, the opening of the filling valves is graduated, these being situated in the upper water reservoir (*banzado*). Thus, a large opening means a greater quantity of water that strikes the paddles of the waterwheel and a greater turning velocity. This in turn increases the angular velocity of the transmission shaft and with it an increased frequency in the striking of the drop hammer. That is, the water is regulated by activating the pull (Fig. 3) from within the smithy (and therefore the mechanism penetrates the roof of the structure), which raises the valve and fills the rectangular conduct. In the case under study, the normal working angular velocity of the waterwheel is 30 rpm, signifying a frequency of 120 strikes per minute of the drop hammer in the forging process (Fig. 5).

The finery forge of Mazonovo has 2 furnaces. The main one is fed with compressed air from the hydraulic trompe and situated next to the drop hammer. The other secondary one serves as a forge, fed with air from a manual bellows.

The second most important aspect in terms of process consists in maintaining a continuous air flow to the furnace to ensure good combustion and high temperatures to soften the

metal to be forged. For this, as opposed to old procedures with manual bellows or by natural ventilation, an invention was used to provide continuous air supply to the furnace.

The first solution for automatic feed to emerge in history was the *barquin*, which took advantage of the movement of the waterwheel to move the bellows. Afterwards, this mechanism was replaced by a more efficient device, which in the literature has different names, such as hydraulic trompe, air trompe or air-blowing tube, but referring to the same mechanism. All this represented a considerable improvement in iron output, as it allowed the blacksmith to make pieces at a production rate far greater than with the previous method. This air-feed system for the furnace was based on the increased velocity reached by the water passing through a choke or funnel in the conduit, which by the Venturi effect lowers the relative pressure, facilitating a draw of outside air through holes (*oídos*) in the trompe (Figs. 6 and 7).

This air mixture in form of bubbles with the water rushes through the vertical conduit of wood (*chifrón*) until reaching a barrel or wind box in the lower part, where it acts as a separation chamber. Here, as the water velocity slows, the pressure increases according to Bernoulli's principle, causing the air bubbles to separate from the water and emerge on the surface. This air is collected in the upper part of the wind box and carried by the wooden conduit towards the furnace of the forge [2]. In the lower part of the wind box a hole allows the water to leave to the outside and into the river. This hole has the form of a siphon, to prevent the air from escaping there. The design of the trompe device determines the air pressure inside the conduit that goes to the furnace [13]. Low in the center of the wind box, a stone slab is placed for the falling water to strike, facilitating the separation of the air from the water, increasing the pressure. Also, this markedly reduces the quantity of air that can escape to the exterior mixed with the water.

Figure 7 shows a diagram of the functioning of the device. Fig. 7a corresponds to the typical trompe of the district of Oscos and by extension north-western Spain, whereas Fig. 7b shows the mallet trompe in the study of Mazonovo in Santa Eulalia, the two differing in the shape of the funnel that causes the acceleration of the water. The main dimensions and geometric characteristics of this device are as follows: the upper tank (1) has a width of 2.3 m, the water inside reaching a height of 1.5 m. The win box (4) has a height of 1 m and a circular cross-section with a diameter of 0.7 m. The distance from the bottom or base of the tank (1) to the top or ceiling of the win box (4) is 2.5 m. The vertical water conduit (3) is quadrangular in cross-section with internal sides measuring 0.2×0.2 m. The funnel (2), which is 0.25 m in length, also has a quadrangular cross-section, its narrowest part measuring 0.12×0.12 m. It has two air inlet holes (7) with a circular cross-section each with a diameter of 0.08 m. The conduit exiting to the forge (6) has a quadrangular internal cross-section of 0.05×0.05 m and is capped at the end by a nozzle with a circular cross-section with a minimum diameter of 2.2 cm. The water outlet to the exterior (8) has a rectangular cross-section measuring 0.10 m wide by 0.07 m high.

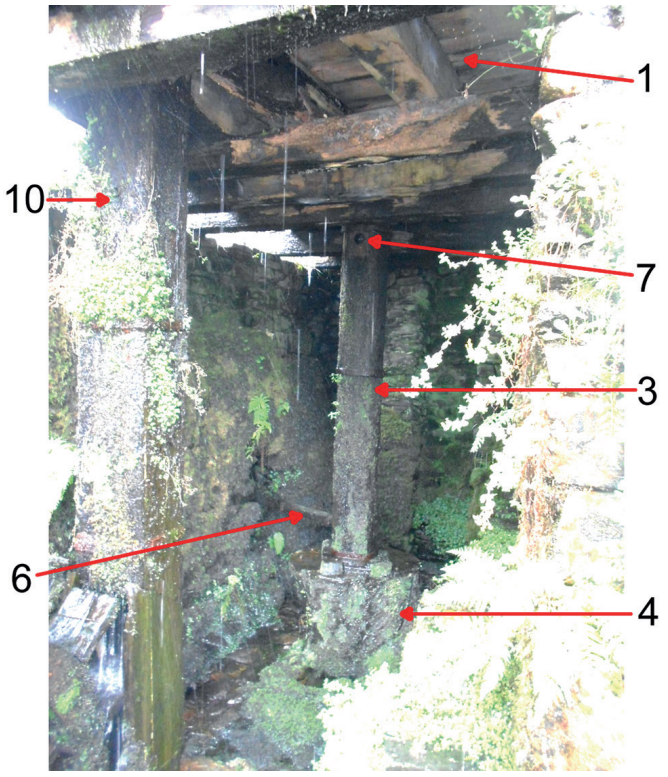

Fig. 6. Detail of the 2 vertical water conduits (the front one to activate the waterwheel, the back one to serve as the hydraulic trompe). Elements: 1) bottom of the wooden water tank, 3) vertical conduit of the trompe, 4) wind box or barrel, 6) wooden pipe carrying air to the forge, 7) entry hole for air, 10) vertical conduit to the waterwheel. The numbering is the same as in Fig. 7

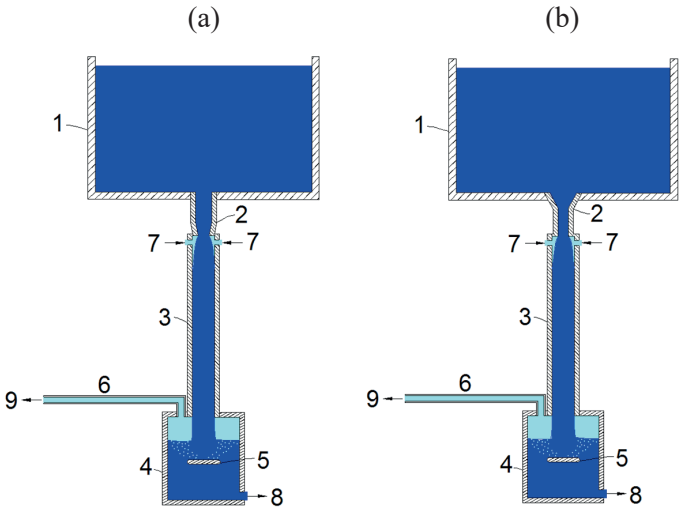

Fig. 7. (a) Schematic longitudinal cross-section of the hydraulic trompe typical of the district of Oscos and (b) mallet trompe at Mazonovo. Elements: 1) upper water reservoir (*banzado*), 2) funnel, 3) vertical conduit (*chifrón*), 4) wind box or barrel, 5) stone slab, 6) air pipe, 7) air inlet holes (*oídos*), 8) water outlet to the exterior (*trapela*), 9) air outlet to the forge

3. Material and Methods

The study of these forging devices began by seeking to determine the functioning parameters through an analysis of their geometry and of the water and air flow. Thus a relationship between the two was established by CFD simulation. Next, to pinpoint the distribution of stress points, the complex device was analyzed using FEA. Data from prior work enabled the mechanics of the forge to be mechanically tested so that the variables of its functioning could be understood.

3.1. 3D modelling. The first step was to model this old forge in order to test the accuracy of the findings. Given that the literature provided no plans or historical documentation of note, empirical methods were used in the field work. Direct measurements were taken, supported by photograms, which gave the dimensions of all the components of the complex structure. After the measurements, the 3D modelling was undertaken using CAD software (parametric Computer-Aided Design), e.g. SolidWorks [14]. The CAD model of the Mazonovo forging device is shown in Fig. 8.

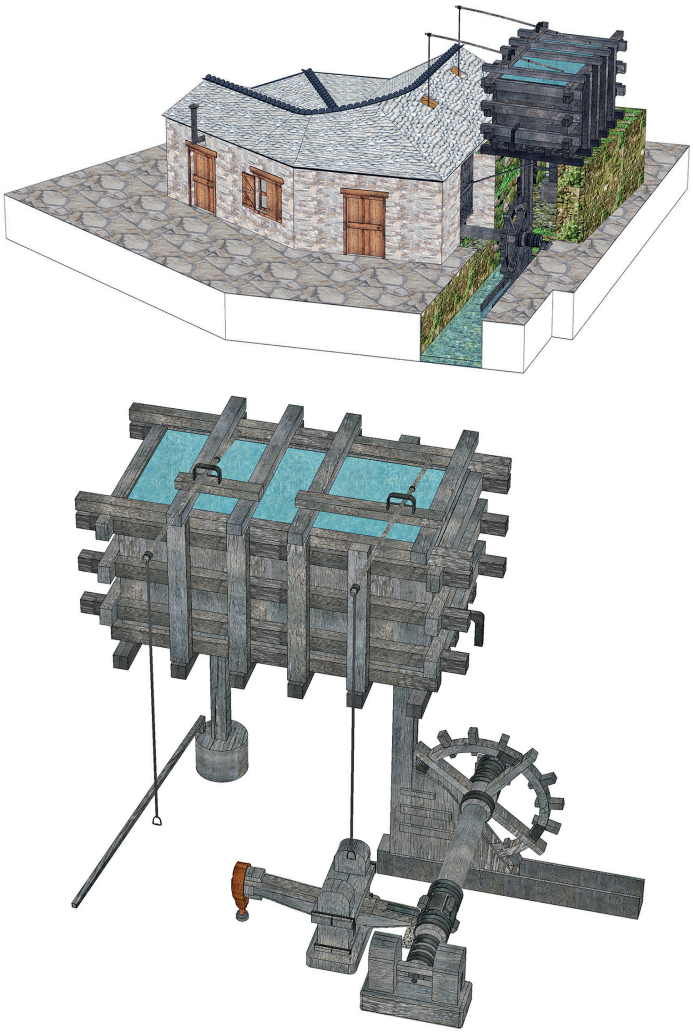

Fig. 8. CAD model of the Mazonovo forging device

3.2. CFD simulation. Next, the flow dynamics of the water-air interaction within the forging device were analyzed. This analysis focused mainly on the hydraulic trompe, which supplies the air to the forge, due to the peculiar characteristics of this device and the major technological advance that it represented for that period. This required a fluid simulation taking into account the real boundary conditions to test the performance of the trompe. Specifically, the CFD technique was used for a computer calculation with the finite volume method (FVM) [15], employing the software Ansys Fluent [16]. At present, CFD is commonly used in engineering fields related to fluids [17–19]. The simulation was intended for determining the air flow to the forge and the pressure carried. The problem of fluid addressed here requires that the boundary conditions and the computational domain be defined in the three-dimensional model being built. In this case, the interior of the trompe constitutes the computational domain.

The own fluid conditions were taken into account. First, the performance of the fluid during the simulation was submitted to governing equations, i.e. the continuity equation expressing the concept that the inflow fluid equaled the outflow and the conservation of the momentum equation. The Reynolds averaged Navier-Stokes (RANS) model was used together with its closure equations [20] in simulating the water and air flow and their mixing within the trompe.

In this model, the variables in the instantaneous Navier-Stokes equations are broken down into two parts: the mean component and a fluctuating component. For the case of velocity, this can be written as:

$$u_i = \bar{u}_i + u_i' \tag{1}$$

where u_i are the components of the velocities in the main directions of the space x_i ($i = 1, 2, 3$), and $\bar{u}_i$ and u_i' are the components of the mean and fluctuating velocities, respectively. The same can be done with other scalar variables such as pressure or energy. This process is known as Reynolds decomposition.

Substituting expressions of this kind for the flow variables in the instantaneous equations, the RANS equations may be formulated as follows:

$$\frac{\partial \rho}{\partial t} + \frac{\partial (\rho u_i)}{\partial x_i} = 0 \tag{2}$$

$$\frac{\partial (\rho u_i)}{\partial t} + \frac{\partial (\rho u_i u_j)}{\partial x_j} = -\frac{\partial p}{\partial x_i} + \frac{\partial}{\partial x_j}\left(\mu\left(\frac{\partial u_i}{\partial x_j} + \frac{\partial u_j}{\partial x_i} - \frac{2}{3}\delta_{ij}\frac{\partial u_l}{\partial x_l}\right)\right) + \frac{\partial}{\partial x_j}\left(-\rho\overline{u_i' u_j'}\right) \tag{3}$$

where, ρ is the density of the fluid, t is time, p is the pressure, μ is the dynamic viscosity, and δ_{ij} is the Kronecker delta function.

We still have more unknowns than equations and hence must model the term $-\rho\overline{u_i' u_j'}$, called Reynolds stresses, with

additional equations. The Boussinesq hypothesis [21] was used to relate the Reynolds stresses to the mean velocity gradients:

$$-\rho\overline{u_i'u_j'} = \mu_t\left(\frac{\partial u_i}{\partial x_j}+\frac{\partial u_j}{\partial x_i}\right)-\frac{2}{3}\left(\rho k+\mu_t\frac{\partial u_k}{\partial x_k}\right)\delta_{ij} \quad (4)$$

where μ_t is the turbulent viscosity.

We used the Realizable k-ε model [22] to close the equation system, where the turbulence is described via two additional variables: k, which is the turbulent kinetic energy, and ε, which represents its rate of dissipation. The transport equations for k and ε in this model are, respectively:

$$\frac{\partial(\rho k)}{\partial t}+\frac{\partial(\rho k u_j)}{\partial x_j}=\frac{\partial}{\partial x_j}\left[\left(\mu+\frac{\mu_t}{\sigma_k}\right)\frac{\partial k}{\partial x_j}\right]+ + G_k - G_b - \rho\varepsilon - Y_M \quad (5)$$

$$\frac{\partial(\rho\varepsilon)}{\partial t}+\frac{\partial(\rho\varepsilon u_j)}{\partial x_j}=\frac{\partial}{\partial x_j}\left[\left(\mu+\frac{\mu_t}{\sigma_\varepsilon}\right)\frac{\partial\varepsilon}{\partial x_j}\right]+\rho C_1 S\varepsilon - - \rho C_2\frac{\varepsilon^2}{k+\sqrt{\nu\varepsilon}}+C_{1\varepsilon}\frac{\varepsilon}{k}C_{3\varepsilon}G_b \quad (6)$$

where

$$C_1=\max\left[0.43,\frac{\eta}{\eta+5}\right],\ \eta=S\frac{k}{\varepsilon},\ S=\sqrt{2S_{ij}S_{ij}} \quad (7)$$

and G_k is the generation of the turbulence kinetic energy due to the mean velocity gradients; G_b represents the generation of turbulence kinetic energy due to buoyancy; Y_M is the contribution of the fluctuating dilatation in compressible turbulence to the overall dissipation rate; ν denotes the kinematic viscosity; C_2, $C_{1\varepsilon}$ and $C_{3\varepsilon}$ are constants; σ_k and σ_ε represent the turbulent Prandtl numbers for k and ε, respectively; and S_{ij} is the mean rate-of-strain tensor.

The turbulent viscosity, μ_t, is calculated by combining k and ε as:

$$\mu_t=\rho C_\mu\frac{k^2}{\varepsilon} \quad (8)$$

C_μ is calculated from

$$C_\mu=\frac{1}{A_0+A_S\frac{kU^*}{\varepsilon}} \quad (9)$$

where $A_0=4.04$, and A_S and U^* are functions of velocity gradients.

$$U^*\equiv\sqrt{S_{ij}S_{ij}+\widetilde{\Omega}_{ij}\widetilde{\Omega}_{ij}} \quad (10)$$

See reference [20] for further details of the meaning of these terms and how to compute them.

One of the approaches that proves most economical for the computation of complex fluid turbulence is provided by RANS models, these serving many engineering purposes with acceptable accuracy. Furthermore, the Realizable k-ε model has been broadly validated for a wide range of flows [23, 24], including free flows such as jets and mixing layers, and separated flows, therefore being very suitable for the case of the flow in the trompe under study here.

Furthermore, in this study two fluids (water and air) were mixed together in certain zones of the trompe and in others separate. The modelling of this situation required a multiphase model, for which the Euler-Euler approach was selected.

In the Eulerian model [20, 25], the phases exist simultaneously. The model treats each one as a separate continuous flow and couples them with interfacial boundary conditions. The coupling between phases takes into account the interfacial exchange of momentum, mass, and energy. It is a complex and sophisticated model that enables modelling both mixed and separate phases.

The conservation equations for each phase contain the monophasic terms as well as interphase terms such as mass transfer, drag, lift, etc., which are generally non-linear and sometimes hinder convergence. This model applies to regimes such as: bubbly flow, droplet flow, particle-laden flow, slurry flow, and fluidized bed.

A parameter commonly used in multiphase flows for the analysis is the volume fraction (α_s), which is the ratio of the volume of phase s (V_s) to the total volume in the cell (V_T), i.e.:

$$\alpha_s=\frac{V_s}{V_T} \quad (11)$$

The mass conservation equation for phase s is:

$$\frac{\partial(\alpha_s\rho_s)}{\partial t}+\nabla\cdot\left(\alpha_s\rho_s\vec{u}_s\right)=\sum_{r=1}^{n}\left(\dot{m}_{rs}-\dot{m}_{sr}\right) \quad (12)$$

where $\vec{u}_s$ is the velocity of phase s, ρ_s denotes the density of phase s, $\dot{m}_{rs}$ represents the mass transfer of the r^{th} to the s^{th} phase, and $\dot{m}_{sr}$ is the mass transfer of the s^{th} to the r^{th} phase.

Likewise, the equation of momentum for phase s is the following

$$\frac{\partial(\alpha_s\rho_s\vec{u}_s)}{\partial t}+\nabla\cdot\left(\alpha_s\rho_s\vec{u}_s\vec{u}_s\right)=-\alpha_s\nabla p+\nabla\cdot\bar{\bar{\tau}}_s+ + \alpha_s\rho_s\vec{g}+\sum_{r=1}^{n}\left(\vec{R}_{rs}+\dot{m}_{rs}\vec{u}_{rs}-\dot{m}_{sr}\vec{u}_{sr}\right)+ + \left(\vec{F}_s+\vec{F}_{lift,s}+\vec{F}_{vm,s}\right) \quad (13)$$

where p is the pressure which is common to all the phases, $\bar{\bar{\tau}}_s$ represents the stress-strain tensor of phase s^{th}, $\vec{g}$ is the gravitational acceleration, $\vec{R}_{rs}$ is the force of interaction between phases r and s, $\vec{u}_{rs}$ and $\vec{u}_{sr}$ denote the interphase velocity, $\vec{F}_s$ represents the external body force, $\vec{F}_{lift,s}$ denotes the lift force,

and $\vec{F}_{vm,s}$ is the virtual mass force. See reference [20] for further details of the meaning of these terms and how to compute them. Finally, the aforecited governing equations were solved using FVM.

The necessary boundary conditions to solve the previously cited equations are shown in Table 1. The turbulent intensity and the hydraulic diameter were used as parameters of turbulence for the k-ε model. The inlets and outlets, both of the air and the water, were established at atmospheric pressure, which was specified by setting the gauge pressure to zero. The turbulent intensity (I_t) was previously estimated by the following formula [16].

$$I_t = 0.16 Re^{-\frac{1}{8}} \tag{14}$$

where Re is the Reynolds number.

Table 1
Boundary conditions for flow simulation in the hydraulic trompe

Air inlet	
Turbulent intensity (%)	4.1
Hydraulic diameter (m)	0.08
Gauge pressure (Pa)	0
Water inlet	
Turbulent intensity (%)	4.3
Hydraulic diameter (m)	1.82
Air outlet	
Backflow turbulent intensity (%)	3.2
Backflow hydraulic diameter (m)	0.022
Gauge pressure (Pa)	0
Water outlet	
Backflow turbulent intensity (%)	2.9
Backflow hydraulic diameter (m)	0.082
Gauge pressure (Pa)	0

The quality of the mesh heavily determines the accuracy of using CFD and, during the calculation, this in turn affects convergence. Here, we refined the mesh close to the critical points of interest. Thus, the density of the mesh was increased below the funnel, at the height of the air inlet holes, and above the stone slab (Fig. 7), to provide better accuracy in these zones, where the air enters and is mixed with the water, and where the air bubbles are released from the water, respectively.

Furthermore, we achieved computational results that were independent of the grid by making mesh studies. In these, we generated and analyzed four mesh resolutions for the trompe, so that the meshes could be compared and verified. The first grid had 668 292 elements, the second 886 421 elements, the third 1 140 216 elements, and the fourth 1 604 325 elements. The air-volume flow rate supplied by the trompe to the forge

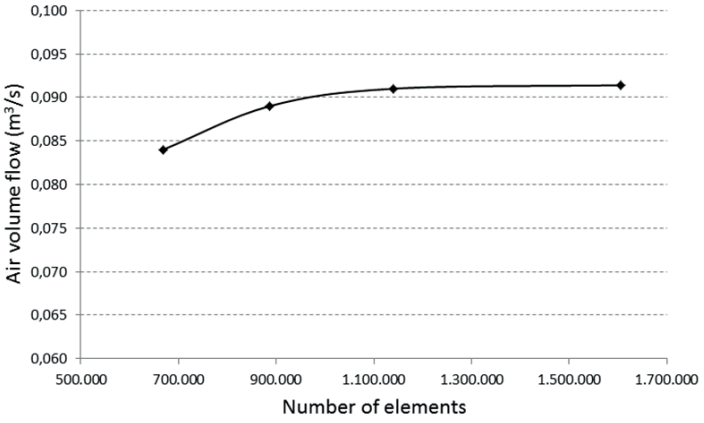

Fig. 9. Effect of CFD mesh resolution on the resulting air-volume flow rate supplied

was chosen as an acceptable criterion to validate the resolution chosen. Fig. 9 shows that, with 1 140 216 and 1 604 325 elements, respectively, the grid sizes clearly gave comparable results. Thus, we conclude from the graph that the results are independent of the grid when a mesh with 1 140 216 or more elements are used, since there is virtually no change in the air-volume flow supplied. With these results, considering the computer resources available, we made the subsequent analyses using a grid of 1 140 216 elements.

3.3. Finite element analysis (FEA). In the final methodological stage, we performed a mechanical analysis of the entire system of movement transmission from the waterwheel to the drop hammer of this finery forge. Analyzing the structure, there are different parts in which it is subject to stresses, from the initial strike of water on the waterwheel to the impact of the drop hammer itself, as well as the transmission of motion from the shaft to the handle of the drop hammer. The study has focused on this last part, as the cam of the transmission shaft is unquestionably the piece that suffers the greatest wear, and hence needs to be replaced more often, due to the heavy blows, continuous stresses and constant friction to which it is subjected [4]. Our basic aim was to establish the distribution of stresses and strains in the cog or cam of the transmission shaft during its impact on the handle of the drop hammer. This impact presents a slight rolling of the cog on the handle. Thus, we may propose an analysis of the stresses and strains on this cog via a static study without excluding approaching the analysis via a dynamic study. To this end, the analysis first required the proper assembly of all the mechanical parts with their correct restrictions. Parametric software was used for the 3D modelling of the motion-transmission system, namely Solidworks. FEA software was then used for the structural analysis, namely Ansys Mechanical [26]. At present, FEA is commonly used in engineering fields [27, 28].

Finally, for the treatment of the geometry, we imported it into the Ansys DesignModeler software [29] from SolidWorks [14] via the STEP format. The software tools of the same family, when integrated by the Ansys Workbench platform [30], offer

finer control and greater speed when the geometric forms and parameters are changed during the tests and simulations. This also provides the most optimal system design.

As to the mathematical fundamentals, we consider that the analysis of the structure is basically a problem of elasticity. If we assume that the different parts are linear elastic bodies, then the linear elastic problem is governed by the following partial differential equations [31, 32]:

– The equilibrium equation based on Cauchy's equation

$$\bar{\bar{\sigma}} \cdot \nabla + \bar{b} = 0 \tag{15}$$

where $\bar{\bar{\sigma}}$ is the stress tensor and $\bar{b}$ is the vector of body forces.

– The constitutive equation derived from the general Hooke's law

$$\bar{\bar{\sigma}} = 2G\left(\bar{\bar{\varepsilon}} + \frac{v}{1-2v}\varepsilon_1 \bar{\bar{I}}\right) \tag{16}$$

where G is the shear elastic modulus, $\bar{\bar{I}}$ is the identity tensor, v is the Poisson's ratio and ε_1 is the first scalar invariant of the tensor.

– The geometric equation that expresses the compatibility relation between infinitesimal strains and displacements

$$\bar{\bar{\varepsilon}} = \frac{1}{2}\left(\bar{u} \otimes \nabla + \nabla \otimes \bar{u}\right) \tag{17}$$

where $\bar{\bar{\varepsilon}}$ is the strain tensor and $\bar{u}$ is the displacement vector.

Considering the boundary of the body divided into two parts $(S = S_u \cup S_t)$, the boundary conditions are:

$$\begin{aligned} \bar{u}\big|_{S_u} &= \overline{u_0} \\ \bar{t}\big|_{S_t} &= \overline{t_0} \end{aligned} \tag{18}$$

where $\overline{u_0}$ and $\overline{t_0}$ are the admissible displacements and loads, respectively.

The procedure for the FEM analysis [31] of the structure starts with the discretization of the body in M finite elements (e) and the union of these elements via different nodes. The approximate displacement field, $\overline{u_e}(\bar{r})$, where $\bar{r}$ is the position vector, is estimated element by element and the approximate strain and stress fields are obtained via the geometric and constitutive equations. Finally, a linear algebraic equation system can be derived by considering the principle of minimum total potential energy and the principle of virtual work. Once the loads or displacements have been defined, this equation system is solved taking into account the boundary conditions, and the approximate nodal displacement field is calculated. The approximate stress and strain fields can also be calculated.

Thus, the potential energy of element π_e is:

$$\begin{aligned} \pi_e = \frac{1}{2}\int_{V_e} \overline{\bar{\sigma}_e}(\bar{r}) : \overline{\bar{\varepsilon}_e}(\bar{r}) dV - \int_{V_e} \overline{u_e}(\bar{r}) \cdot \bar{b} dV - \\ - \int_{S_{et}} \overline{u_e}(\bar{r}) \cdot \bar{t} dS. \end{aligned} \tag{19}$$

The above equation can be expressed with matrix products and introducing vectors instead of tensors [31, 32]:

$$\begin{aligned} \pi_e = \frac{1}{2}\int_{V_e} \left[\overline{\varepsilon_e}(\bar{r})\right]^T \overline{\sigma_e}(\bar{r}) dV - \int_{V_e} \left[\overline{u_e}(\bar{r})\right]^T \bar{b} dV - \\ - \int_{S_{et}} \left[\overline{u_e}(\bar{r})\right]^T \bar{t} dS. \end{aligned} \tag{20}$$

As stated above, the strain and stress fields are obtained as $\overline{\varepsilon_e}(\bar{r}) = \bar{\bar{\partial}}\,\overline{u_e}(\bar{r}) = \overline{\bar{B}_e}(\bar{r}) \cdot \bar{u}_e$ and $\overline{\sigma_e}(\bar{r}) = \bar{\bar{C}}\,\overline{\bar{B}_e}(\bar{r}) \cdot \bar{u}_e$ respectively, where $\overline{\bar{B}_e}(\bar{r}) = \bar{\bar{\partial}}\,\overline{\bar{N}_e}(\bar{r})$ is the product of the differential operator and the matrix of shape functions, and $\bar{\bar{C}}$, the constitutive matrix including material constants. Hence, the stiffness matrix can be defined as:

$$\overline{\bar{K}_e} = \int_{V_e} \left[\overline{\bar{B}_e}(\bar{r})\right]^T \bar{\bar{C}}\,\overline{\bar{B}_e}(\bar{r}) dV. \tag{21}$$

Finally, by adding the potential energy of all the elements $\left(\Pi = \sum_{e=1}^{M} \pi_e\right)$ and applying the principle of virtual work $(\delta\Pi = 0)$ to the entire body, then a linear algebraic equation system can be derived with respect to the nodes [31]:

$$\bar{\bar{K}}\,\overline{U} = \overline{F} \tag{22}$$

where $\bar{\bar{K}}$ is the stiffness matrix of the body, $\overline{U}$ is the nodal displacement vector and $\overline{F}$ is the nodal force vector.

Ansys solves the above equation system by determining the displacement vector and different parameters that show the behavior of the structure, such as stress and strain, in addition to safety factors based on the structural characteristics derived from the material.

Different previous considerations must be made to perform the analysis. The motion-transmission system should guarantee a striking frequency of the drop hammer sufficient for the smelting process. This frequency depends directly on the angular velocity of the waterwheel. In this case, the measurements made gave a mean angular-velocity value of 30 rpm, representing a frequency of 120 blows per minute of the drop hammer. These data, after the CAD modelling, were compared with a motion analysis by the software SolidWorks Motion. This simulation did not permit a comparison of the real data but rather verified the geometry, spatial arrangement, and geometric relations of the CAD model itself. After this geometry was validated by the motion analysis and once the angular velocity and the mass of the components were known, the structural analysis of the motion-transmission system was undertaken.

Within the possibilities that Ansys offers for structural analysis, a static analysis was chosen in the case in hand, validated through three different scenarios, based on the actual functioning of the transmission system. In each rotation of the waterwheel (and thus of the transmission shaft), one of the four cams strikes, with a slight rolling, the handle of the drop hammer downwards, after which it leaves this position, not returning to it until the following rotation. If the waterwheel

is stopped at this instant, when one of the cams strikes the ensemble formed by the handle and the drop hammer, it would have the most delicate position of the entire rotation from the structural standpoint. Furthermore, it should be noted that this position is repeated four times with each revolution, alternating cams each time. This position of equilibrium allows us to statically analyze the cam that impacts on the handle of the drop hammer, proposing several scenarios:

a) The system is in equilibrium subject only to gravity and defining contact between the cam and the handle.
b) The system is in equilibrium subjected to a force applied directly on the cam. This force can be obtained by considering $\sum M = 0$ with respect to the axis of rotation of the drop hammer handle.
c) The transmission system is subject to gravity and a load associated with the rotation of the waterwheel, defining contact between the cam and the handle. Said load will vary in a short time interval, 0.0005 seconds, and is expressed as the rotation the waterwheel (and hence the shaft) undergoes in this interval with respect to its centers of rotation.

Scenarios a) and c) should provide similar results, as they consider the same initial conditions, replacing the effect of the handle and the hammer through its contact with the cam by an equivalent force. Scenario c) adds a simulation of the rotation at the instant the cam rolls on the handle to these effects. Consequently, three different static studies were carried out to validate and compare the results, proposing two equilibrium scenarios and another in which a load is applied in a short time interval, which may be considered quasi-dynamic.

Each of the scenarios was analyzed in Ansys Mechanical under the initial considerations and conditions shown in Table 2.

Table 2
Summary of initial considerations and conditions in the FEA of the different scenarios

Materials	
Wrought iron – Isotropic	
Density (kg m-3)	7200
Young's Modulus (MPa)	1.1E+05
Tensile Ultimate Strength (MPa)	240
Oak – Orthotropic	
Density (kg m-3)	560
Young's Modulus X (MPa)	11000
Young's Modulus Y (MPa)	730
Young's Modulus Z (MPa)	730
Tensile Ultimate Strength (MPa)	117
Compressive Ultimate Strength (MPa)	59
Assignment of the material The orthotropic material is assigned to each element of the assembly so that the X direction coincides with the direction of the grain of the wood. In the case of the cam, the X direction is perpendicular to the longitudinal axis of the handle (see Figs. 16 and 17).	
Scenario A	
Loads Standard Earth Gravity.	
Contacts and Joints Fixed joints and bonded contact between the cam and the handle.	
Scenario B	
Loads – Standard Earth Gravity. – Force obtained by applying with respect to the axis of rotation of the drop hammer handle. F = 1660.6 Newtons	
Contacts and Joints Fixed joints and Bonded contacts. No contact exists between the cam and the handle.	
Scenario C	
Loads – Standard Earth Gravity. – Joint Load equivalent to a rotation in the joint of 30 rpm. This is applied progressively for a period of 0.0005 seconds in which it is assumed that the contact between the cam and the handle remains stable.	
Contacts and Joints Revolute joints and Bonded contact between the cam and the handle.	

4. Results and Discussion

This study offers notable results for each methodological stage. First, in the field work, data on the geometry of the parts was compiled for the finery forge. This information was used to build 3D models with the use of the aforementioned software (Fig. 8). This had two purposes: first for the permanent recording and storage of the 3D geometric records; and second to build parametrized ensembles to serve the mechanical analysis of the overall device.

The geometry established was used to test the water and air flow interacting through the hydraulic trompe analyzed using CFD. In this way, we determined the air-volume flow rate supplied by the trompe to the forge. With respect to the boundary conditions, as already stated, atmospheric pressure was assigned to the top of the water reservoir or *banzado*, to the air inlet holes or *oídos*, to the water outlet to the outside, and to the air outlet to the forge.

The CFD simulation shows that the maximum air-volume flow rate supplied by the trompe is 0.091 m^3/s in the Mazonovo forge. This value is given when the maximum water flow is allowed to pass through the trompe. This result agrees well with other experimental works on ancient forging devices [33, 34]. We have also carried out similar simulations with other forges of the Oscos district (Fig. 7), and comparable results were found for the flow supplied $(0.096\ m^3/s)$. Thus, we conclude that the design of the funnel is not decisive to determine the flow rate of air drawn in by the falling water stream, so long as certain basic parameters are followed.

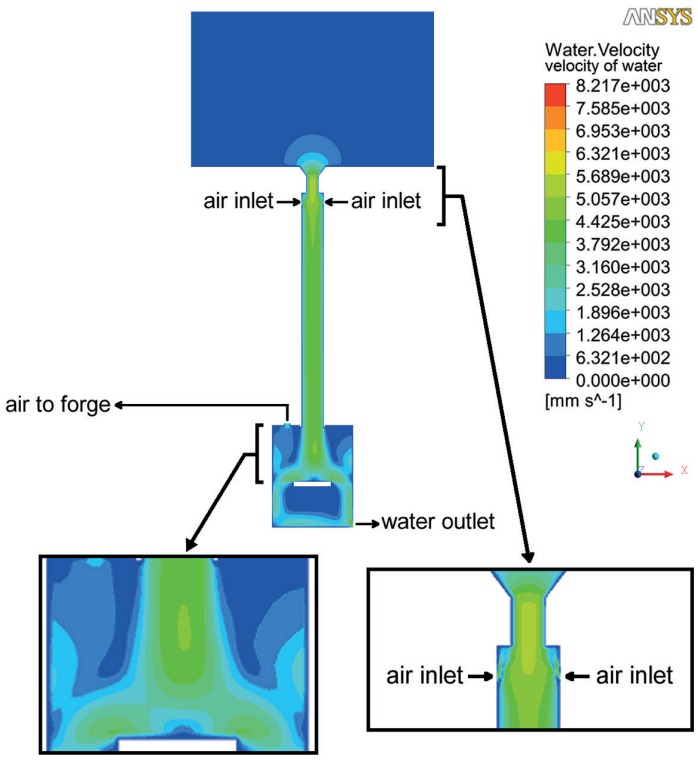

Fig. 10. CFD simulation of the spatial distribution of the velocity of water

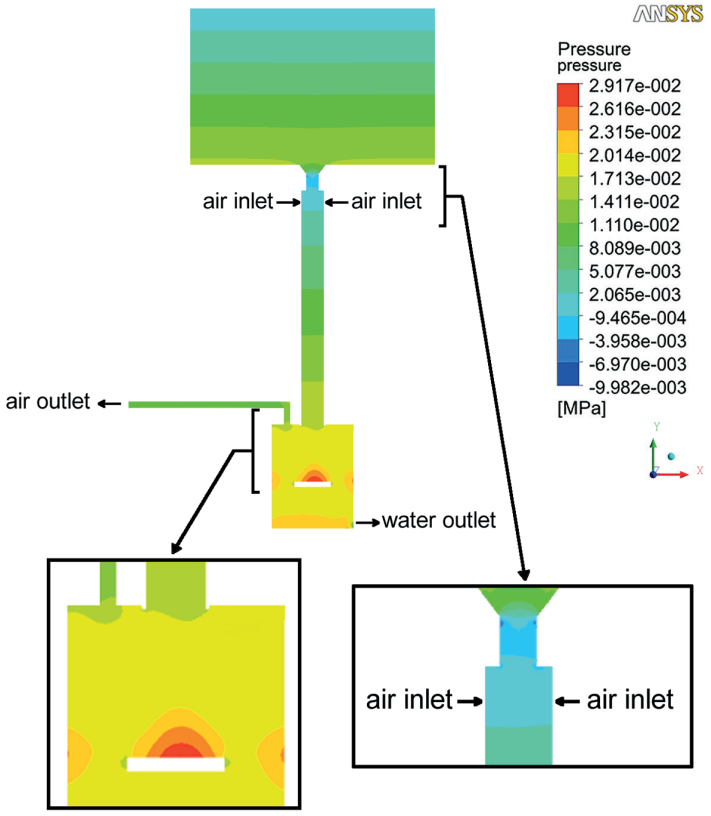

Fig. 11. CFD simulation of the spatial distribution of the pressures of both fluids (water and air)

Figure 10 shows the result of the simulation of the spatial distribution of the velocity of water determined in the interior of the trompe of Mazonovo forge, Fig. 11 depicts the distribution of the pressures of both fluids (water and air), in one zone mixed and in others separated, and Fig. 12 presents the distribution of the volume fraction of air (see Eq. 11).

In these figures, it can be seen that the velocity of the water increases below the funnel, at the height of the air inlet holes (Fig. 10). This causes the relative pressure to fall below atmospheric pressure (Fig. 11), which leads to air being sucked in through the holes (Fig. 12). This is what is known as the Venturi effect.

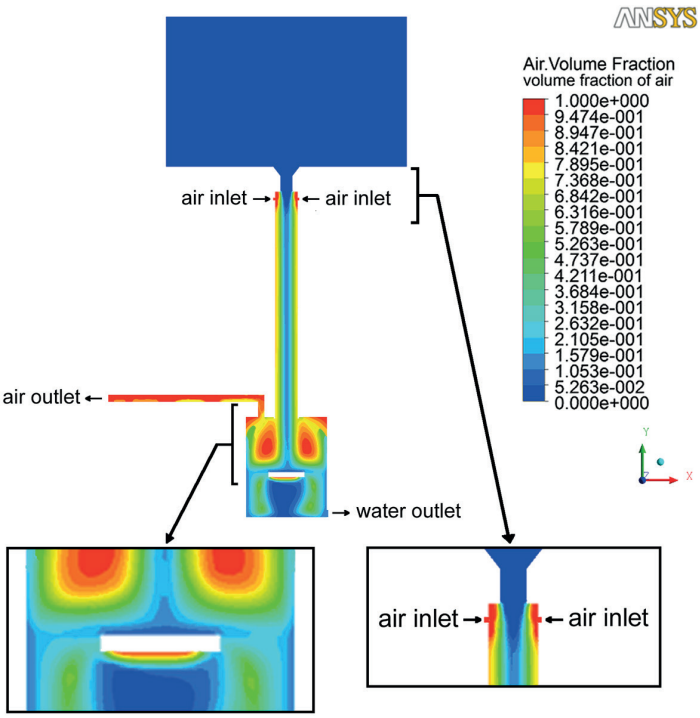

Fig. 12. CFD simulation of the spatial distribution of the volume fraction of air

Above the stone slab can be seen an area of points where the velocity approaches zero, i.e. quasi-stagnation points (Fig. 10). This leads to an increase in pressure that reaches a maximum (Fig. 11) and facilitates the release of air bubbles. As the water strikes here, most of it goes towards the side walls of the barrel, where, as it strikes against the barrel at the same height, quasi-stagnation zones of maximum pressure appear that once more facilitate the release of the bubbles.

Also, as a means of offering fuller information on the functioning range of this hydraulic device, the graph in Fig. 13 depicts the volume flow rate of air supplied by the trompe for different distances from the air inlet holes (*oídos*) to the funnel, while Figs. 14 and 15 show the air-volume flow rate supplied by the trompe for different funnel and vertical conduit widths, respectively. In Fig. 14, we consider the minimum width as the reference.

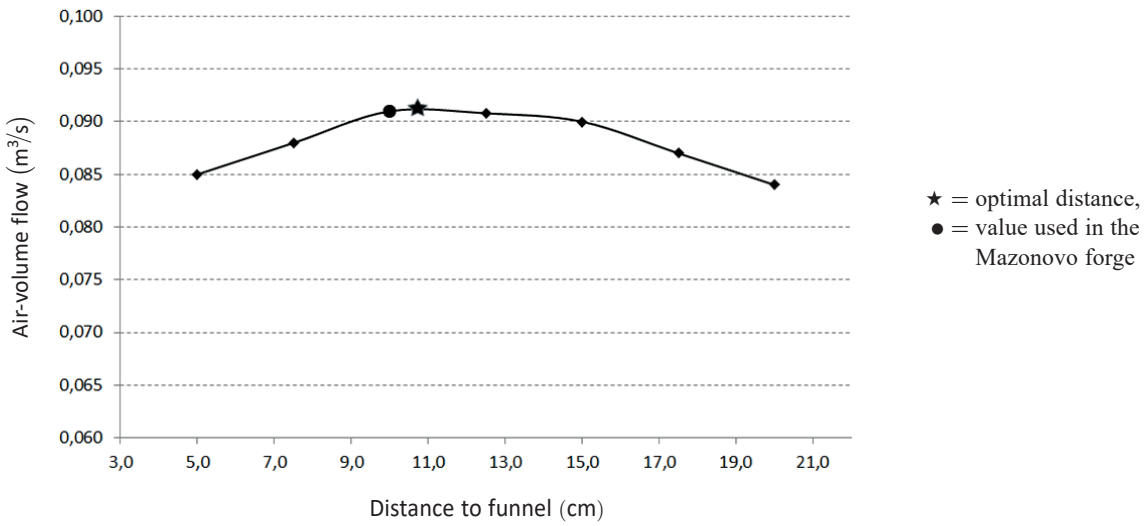

Fig. 13. Air-volume flow rate supplied by the trompe for different distances from the air inlet to the funnel

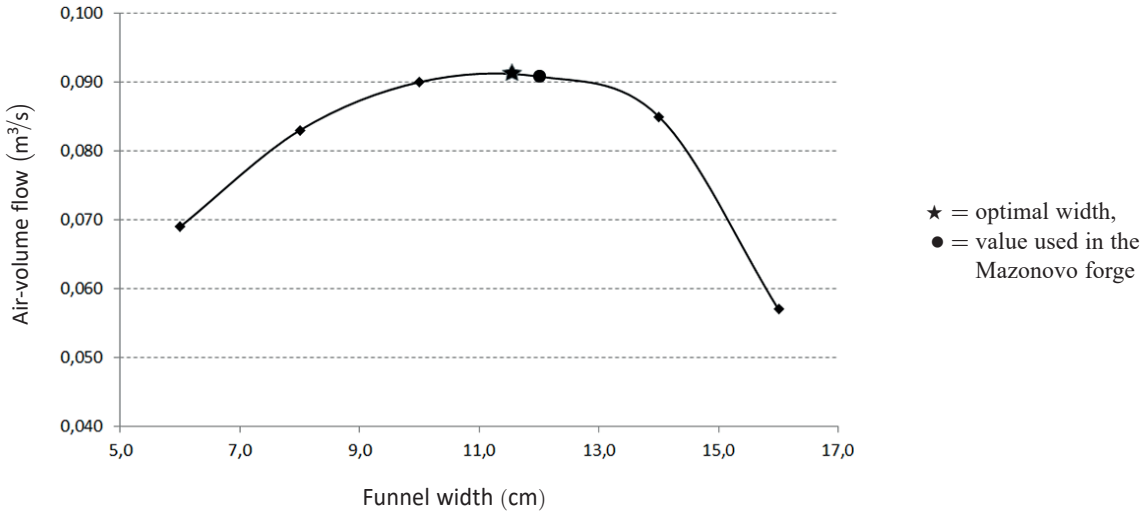

Fig. 14. Air-volume flow rate supplied by the trompe for different funnel widths

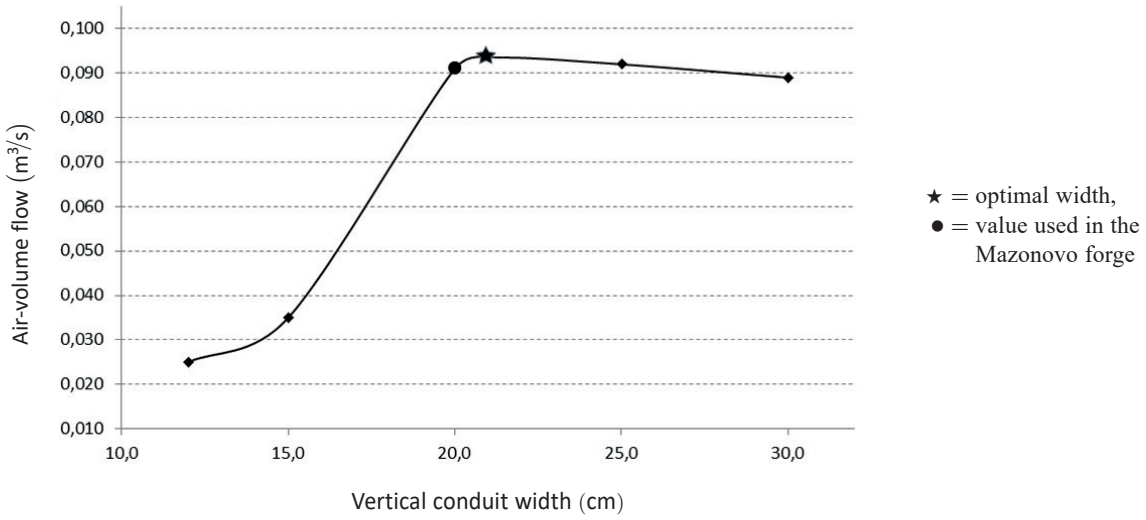

Fig. 15. Air-volume flow rate supplied by the trompe for different vertical conduit widths.

In the case of the Mazonovo forge, the distance from the air inlet to the funnel is 10 cm, the minimum width of the funnel is 12 cm and the width of the vertical conduit of the trompe is 20 cm. These graphs indicate that these values correspond to the optimal zones, i.e. the maximum air-volume flow supply. Surprisingly in that period, in which current analysis tools were not available, over years of trial and error, optimal operating values were found and they coincide with those that we confirm in the present CFD analysis, reflecting the skills of those technicians.

On the other hand, the water consumption from the river to maintain the trompe functioning depended directly on the minimum width of the funnel, so that with lower values this minimum width would consume less water. The CFD analysis reveals that this width can be reduced to 10 cm and maintain almost the same air flow to the forge. That is, with 12 cm of width, 0.143 m^3/s of water is consumed, while at 10 cm the consumption is 0.117 m^3/s. This is a considerable saving, which is important because many trompe could not be used in summer during the month or months of greatest drought, since the water carried by the river was not sufficient to maintain the waterwheel and the trompe moving at the same time. In this case, the usual practice was to close the trompe so that all the water flowed to the wheel, as the motion of the drop hammer took priority, and during this time the trompe was replaced by a manual bellows. As a result of the CFD analysis, the trompe could be redesigned so that this period could be reduced by needing less water to function.

Next, the results of the material mechanical resistance are examined making up the entire motion-transmission system from the waterwheel to the drop hammer of this finery forge with respect to the forces encountered in daily use. The study focuses especially on the cam that strikes the handle of the drop hammer, as it is the part of the entire system that is most subject to wear.

As mentioned above in Table 2, the starting data for the analysis were different for each scenario, where the conditions of the study and the applied loads vary. The properties of the material of the components of the motion-transmission system will, however, be the same in the different scenarios.

As already mentioned, in order to test and validate the static assumption and the results thus obtained, three static analyses were carried out using FEA in which the distribution of stresses, the total deformation, and the safety factor in the transmission system were analyzed, paying particular attention to the cam during its impact, with a slight rolling, on the drop hammer handle. The results are shown in Figs. 16 and 17 and are summarized in Table 3. The first of the proposed scenarios was

Table 3
Summary of the FEA results

Results	
Scenario A	
Maximum Stress (MPa) – Cam	2.89
Maximum Deformation (mm) – Drop Hammer	0.39
Maximum Deformation (mm) – Cam	0.09
Minimum Safety Factor	>10
Compressive Ultimate Strength	
Scenario B	
Maximum Stress (MPa) – Cam	2.80
Maximum Deformation (mm) – Wheel	0.41
Maximum Deformation (mm) – Cam	0.17
Minimum Safety Factor	>10
Compressive Ultimate Strength	
Scenario C	
Maximum Stress (MPa) – Cam	7.50
Maximum Deformation (mm) – Wheel	1.75
Maximum Deformation (mm) – Cam	0.35
Minimum Safety Factor	>7.5
Compressive Ultimate Strength	

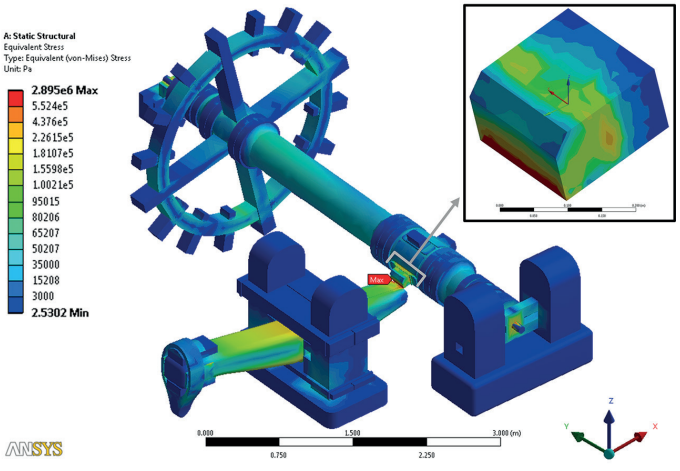

Fig. 16. Distribution of stresses in the motion-transmission system of the forge, highlighting the effects on the cam

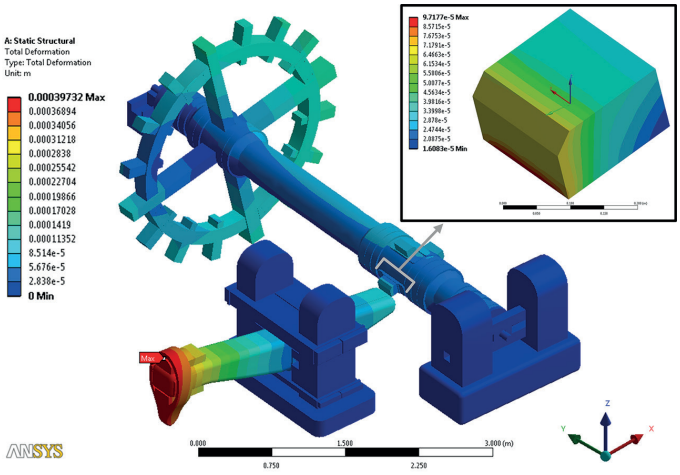

Fig. 17. Total deformation in the motion-transmission system of the forge highlighting the effects on the cam

chosen for the images because it considers the basic equilibrium scenario, whereas all the scenarios appear in the table.

The motion-transmission system of this forge, as indicated above, is made mainly from oak. The most unfavorable maximum admissible stress for this wood is that of parallel-to-grain compression, this reaching 59 MPa [35]. As can be deduced from the results presented in Table 3, which provides the maximum values analyzed in the structure, there are no points in the wooden parts that reached or even approached the maximum stress value. From the results obtained, it can be concluded that:

- In Scenario A, which we consider one of basic equilibrium, the greatest stress of the system reached 2.89 MPa, this being in the cams of the transmission shaft. This was the component that transmitted motion and force to the next element of the system, the handle of the drop hammer. In the other scenarios, the stresses at this critical point were also measured, the stress remaining below half of the maximum admissible work stress in all cases.
- The static analysis proposed in Scenarios A and B is consistent with the assumptions of static equilibrium, as the results of Scenarios A and B are similar (2.89 versus 2.80 MPa). In both cases, the values are much lower than the material limits.
- The analysis of Scenario C provides higher results, with a value of 7.50 MPa on the cam. This scenario considers a quasi-dynamic case, in which the rotation speed of the shaft is verified through Solidworks Motion. The increase is due to the assumption of the impact between the cam and the handle, considered as a progressive load during the instant it lasts. Even with these assumptions, the maximum results are well below the material limits. Furthermore, they are consistent with reality, as they indicate that the cam is subject to continuous stresses during the transmission process due to the heavy blows, continuous stresses. and constant friction to which it is subjected. This means greater wear and hence the need to replace the piece more often than any other part of the system. The 4 cams do not usually wear out at the same time, causing variations in the frequency at which the drop hammer strikes.
- The material assigned to the cam (and to the other elements of the structure made of wood) is oak, which behaves orthotropically. The greatest strength is found in the direction of the grain, which favors its structural behavior. The cam is positioned in such a way that the direction of its grain is parallel to its housing and hence perpendicular to the longitudinal axis of the handle of the drop hammer. This feature of the placement guarantees greater rigidity and durability of the piece. To verify this assumption, it suffices to modify the assignment of the coordinate system to the material to appreciate these effects and observe an increase in the stresses and the consequent decrease in the safety margins. For example, in Scenario C this change results in the maximum stress on the cam varying from 7.50 MPa to 10.78 MPa.

The above results are not surprising, as the cams were small in comparison to the other components of the system. The cams transmitted all the force exerted by the water on the waterwheel to the next component. This concentrated all the force within the system and thus raised the stress on the cams. Nevertheless, this maximum stress did not reach the force necessary to break the material making up the cams (oak wood). This finding is consistent with other reports using FEA methods in other ancient structures [36], where high safety coefficients have also been found. These safety margins could have been the result of those builders being unable to calculate the optimal stresses of a structure and therefore their primary goal was to ensure the endurance of the system.

Another element where stresses were high, but not as extreme as in the above-mentioned case, was the internal support of the transmission shaft, where stress reached around 0.72 MPa in Scenario A and 1.74 MPa in Scenario C, which is more realistic due to the movement in the revolute joint.

However, this support as well as the one on which the handle of the drop hammer pivots received strong reinforcement with added material. Furthermore, the lodging of the cams in the shaft was covered with three pieces of iron (*xemelas*) for isolation and protection. Similarly, the space of the transmission shaft between the teeth was covered with a strip of iron (*bandeta*) to reinforce that area. Those points received less stress because of the reinforcement, preventing values that could lead to breakage, The support elements for the transmission shaft as well as the piece on which the handle rotated were joined with large logs (*cepos*) set belowground, offering solidity and stability to the entire structure.

5. Conclusions

The present work provides analyses on the geometrical, mechanical, and hydraulic performance of an old forging device in Mazonovo, near the town of Santa Eulalia de Oscos (Asturias province, Spain). This is one of the prime historical examples of a finery forge still operating in Spain. The aim is to contribute to the recovery of such remarkable instances of Spanish historical and ethnological heritage.

This study used rigorous methodology involving *ad hoc* research employing three basic tools: 3D documentation, CFD simulation of water and air interaction in the forge, focusing primarily on the study of the hydraulic trompe that supplies the air to the forge; and finally an FEA analysis of the motion-transmission system of the forge to determine critical stress points.

The CFD analysis revealed that certain parameters of importance in the design of the trompe have optimal values; that is, that they provide a maximum supply of air-volume flow to the forge. Surprisingly in a period without current analysis means, the trail-and-error method provided optimal values, which coincide with those confirmed in the CFD analysis made. Nevertheless, the study did indicate, although in that period such calculations were not possible, that this new technology reduced water consumption by maintaining the air flow to the forge similar or with a negligible reduction, implying the possibility of using the trompe for more time during droughts, i.e. in the summer months.

Regarding stress and its spatial distribution throughout the motion-transmission system, the cams of the camshaft under-

went the greatest concentration, transmitting the movement and force to handle of the drop hammer. Nevertheless, the stress values did not reach 50% of the maximum admissible work stress. The oak-wood performance was excellent, as maximum stress was not reached at any point of the ensemble.

The findings agree with those provided by the blacksmith who works with this finery forge, and with data available in the literature of forges of similar characteristics, thus validating the methodological use of 3D modelling, CFD, and FEA, in the present study.

Acknowledgements. The authors would like to thank Friedrich Bramsteidl, the Mazonovo forge blacksmith, for his valuable comments and cooperation in this study. Thanks are also due to Antonio Riveiro Rodríguez for his help in this matter.

References

[1] C. Vázquez-Cáceres, "The drop hammer in Navafría for working copper", in *Una mirada a nuestro patrimonio industrial*, pp. 65–81, Madrid, Colegio Oficial de Ingenieros Industriales, 2010 [in Spanish].
[2] G. Morís Menéndez-Valdés, *Historical hydraulic engines: mills, fulling mills and finery forges*, Oviedo, Colegio Oficial de Ingenieros Industriales de Asturias y León, 2001 [in Spanish].
[3] I. González-Tascón, *Spanish hydraulic factories*, Madrid, Ministerio de Obras Públicas y Urbanismo, 2004 [in Spanish].
[4] P. Quintana-López, The tillage and artisanal transformation of iron in Taramundi and the Oscos. Centuries XVI–XXI. Contribution to its knowledge, Oviedo, Asociación Cultural "Os Castros" de Taramundi, 2005 [in Spanish].
[5] J. Caro-Baroja, *Spanish popular technology*, Madrid, Galaxia Gutenberg, 1996 [in Spanish].
[6] L. Rodríguez-Castellano, "Popular iron industry: the drop hammer", *Boletín del Real Instituto de Estudios Asturianos*, 8, 294–315 (1954) [in Spanish].
[7] R. Casado and J.M. Carrascosa, "The copper boiler making and the drop hammer in Abán de Navafría", *Narria* 6, 21–24 (1977) [in Spanish].
[8] A.M. Irisarri and A. Pelayo, "Failure analysis of an open die forging drop hammer", *Eng. Fail. Anal.* 16, 1727–1733 (2009).
[9] J.I. Rojas-Sola, J. Suárez-Quirós, and R. Rubio-García, "The tradition of fulling mills: a study from engineering", *Interciencia* 32 (10), 675–678 (2007) [in Spanish].
[10] Etnographic place of Mazonovo, https://www.turismoasturias.es/en/descubre/cultura/museos-y-espacios-culturales/otros-espacios/conjunto-etnografico-de-mazonovo, (Access online: 10.06.2018).
[11] Mazonovo drop hammer, https://www.youtube.com/watch?v=NWySMSzxjN4, (Access online: 10.06.2018) [in Spanish].
[12] M. Denny, "The efficiency of overshot and undershot waterwheels", Eur. J. Phys. 25, 193–202 (2004).
[13] J.R. Hunt, "Harness hydro power with a trompe: Learn how to use water pressure to make free compressed air", *Mother Earth News,* http://www.motherearthnews.com/renewableenergy/hydro-power-zmaz77jazbon, (Access online: 10.06.2018).
[14] SolidWorks Manual, Suresnes, Dassault Systèmes, 2017.
[15] L. Li, J. Sun, and Y. Li, "Thermal load and bending analysis of heat collection element of direct-steam-generation parabolic-trough solar power plant", *Appl. Therm. Eng.* 127, 1530–1542 (2017).
[16] ANSYS Fluent User's Guide, Canonsburg, Ansys Inc., 2017.
[17] A. Menéndez-Díaz, C. Ordóñez-Galán, J.B. Bouza-Rodríguez, and J.J. Fernández-Calleja, "Thermal analysis of a stoneware panel covering radiators", *Appl. Energy* 131, 248–256 (2014).
[18] S. Gepner, J. Majewski, and J. Rokicki, "Parallel anisotropic mesh refinement with dynamic load balancing for transonic flow simulations", *Bull. Pol. Ac.: Tech.* 65(2), 195–207 (2017).
[19] D. Gawel, M. Nowak, H. Hausa, and R. Roszak, "New biomimetic approach to the aircraft wing structural design based on aeroelastic analysis", *Bull. Pol. Ac.: Tech.* 65(5), 741–750 (2017).
[20] ANSYS Fluent Theory Guide, Canonsburg, Ansys Inc., 2017.
[21] J.O. Hinze. Turbulence. McGraw-Hill Publishing Co., New York, 1975.
[22] T.H. Shih, W.W. Liou, A. Shabbir, Z. Yang, and J. Zhu, "A new k-ε eddy viscosity model for high Reynolds number turbulent flows", *Comput. Fluids* 24(3), 227–238 (1995).
[23] X.P. Gao, H. Zhang, J.J. Liu, B.W. Sun, and Y. Tian, "Numerical investigation of flow in a vertical pipe inlet/outlet with a horizontal anti-vortex plate: effect of diversion orifices height and divergence angle", *Eng. Appl. Comp. Fluid Mech.* 12(1), 182–194 (2017).
[24] W.W. Kim, D. Choudhury, and B. Patel, "Computations of complex turbulent flows using the commercial code ANSYS Fluent", in *Proceedings of the ICASE/LARC/AFOSR Symposium on Modeling Complex Turbulent Flows*, Hampton, Virginia, 1997.
[25] C. Crowe, M. Sommerfield, and Y. Tsuji, Multiphase flows with droplets and particles, CRC Press, London (1998).
[26] ANSYS Mechanical User's Guide, Canonsburg, Ansys Inc., 2017.
[27] K. Michalczyk, "Natural transverse vibrations of helical springs in sections covered with elastic coatings", *Bull. Pol. Ac.: Tech.* 65(6), 949–959 (2017).
[28] M. Rucka, W. Witkowski, J. Chróścielewski, S. Burzyński, and K. Wilde, "A novel formulation of 3D spectral element for wave propagation in reinforced concrete", *Bull. Pol. Ac.: Tech.* 65(6), 805–813 (2017).
[29] DesignModeler User's Guide, Canonsburg, Ansys Inc., 2017.
[30] Workbench User's Guide, Canonsburg, Ansys Inc., 2017.
[31] I. Moharos, I. Oldal, and A. Szekrényes, *Finite Element Methode*, Budapest, Typotex Publishing House, 2012.
[32] X. Oliver, and C. Agelet de Saracibar, *Continuum Mechanics for Engineers. Theory and Problems*, 2nd Edition, 2017.
[33] V. Fuses i Navarra, *Noves aplicacions de la trompa d'aigua o trompa dels Pirineus: Elevació d'aigua, aire comprimit i generació d'electricitat*, Dissertation, Technical University of Catalonia, 2010, https://upcommons.upc.edu/handle/2117/93627. (Access online: 10.06.2018).
[34] R. Bosch i Tous, and V. Fuses i Navarra, *La trompa de agua o trompa de los Pirineos. Recuperación del principio funcional para aplicaciones de bombeo. Aproximación mediante las ecuaciones electromagnéticas,* Dissertation, Technical University of Catalonia, 2010, http://aedie.org/11chlie-papers/248-Bosch.pdf, (Access online: 10.06.2018).
[35] T. Volkmer, T. Lorenz, P. Hass, and P. Niemz, "Influence of heat pressure steaming (HPS) on the mechanical and physical properties of common oak wood", *Eur. J. Wood Wood Prod.* 72(2), 249–259 (2014).
[36] J.I. Rojas-Sola, J.B. Bouza-Rodríguez, and A. Menéndez-Díaz, "Technical and functional analysis of Spanish windmills: 3D modeling, computational-fluid dynamics simulation and finite-element analysis", *Energy Conv. Manag.* 123, 130–139 (2016).